



**HAL**  
open science

## **TiO<sub>2</sub>-SiO<sub>2</sub> mixed oxide deposited by low pressure PECVD: Insights on optical and nanoscale electrical properties**

Maria Mitronika, C Villeneuve-Faure, F Massol, Laurent Boudou, W Ravisy, M P Besland, A Goulet, M Richard-Plouet

► **To cite this version:**

Maria Mitronika, C Villeneuve-Faure, F Massol, Laurent Boudou, W Ravisy, et al.. TiO<sub>2</sub>-SiO<sub>2</sub> mixed oxide deposited by low pressure PECVD: Insights on optical and nanoscale electrical properties. Applied Surface Science, 2021, 541, 10.1016/j.apsusc.2020.148510 . hal-03449033

**HAL Id: hal-03449033**

**<https://hal.science/hal-03449033>**

Submitted on 25 Nov 2021

**HAL** is a multi-disciplinary open access archive for the deposit and dissemination of scientific research documents, whether they are published or not. The documents may come from teaching and research institutions in France or abroad, or from public or private research centers.

L'archive ouverte pluridisciplinaire **HAL**, est destinée au dépôt et à la diffusion de documents scientifiques de niveau recherche, publiés ou non, émanant des établissements d'enseignement et de recherche français ou étrangers, des laboratoires publics ou privés.

## Journal Pre-proofs

Full Length Article

TiO<sub>2</sub>-SiO<sub>2</sub> mixed oxide deposited by low pressure PECVD: insights on optical and nanoscale electrical properties

M. Mitronika, C. Villeneuve-Faure, F. Massol, L. Boudou, W. Ravisy, M.P. Besland, A. Gouillet, M. Richard-Plouet

PII: S0169-4332(20)33268-2  
DOI: <https://doi.org/10.1016/j.apsusc.2020.148510>  
Reference: APSUSC 148510

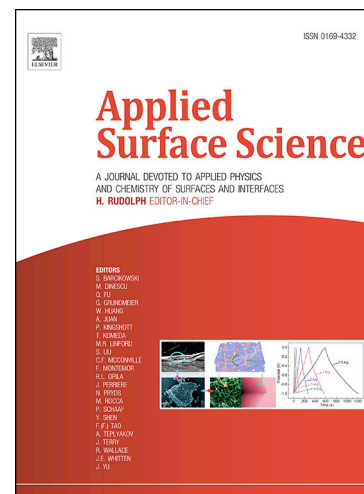
To appear in: *Applied Surface Science*

Received Date: 21 September 2020  
Revised Date: 13 November 2020  
Accepted Date: 15 November 2020

Please cite this article as: M. Mitronika, C. Villeneuve-Faure, F. Massol, L. Boudou, W. Ravisy, M.P. Besland, A. Gouillet, M. Richard-Plouet, TiO<sub>2</sub>-SiO<sub>2</sub> mixed oxide deposited by low pressure PECVD: insights on optical and nanoscale electrical properties, *Applied Surface Science* (2020), doi: <https://doi.org/10.1016/j.apsusc.2020.148510>

This is a PDF file of an article that has undergone enhancements after acceptance, such as the addition of a cover page and metadata, and formatting for readability, but it is not yet the definitive version of record. This version will undergo additional copyediting, typesetting and review before it is published in its final form, but we are providing this version to give early visibility of the article. Please note that, during the production process, errors may be discovered which could affect the content, and all legal disclaimers that apply to the journal pertain.

© 2020 Published by Elsevier B.V.



# TiO<sub>2</sub>-SiO<sub>2</sub> mixed oxide deposited by low pressure PECVD: insights on optical and nanoscale electrical properties

M. Mitronika<sup>1</sup>, C. Villeneuve-Faure<sup>2</sup>, F. Massol<sup>2</sup>, L. Boudou<sup>2</sup>, W. Ravisy<sup>1</sup>, M.P. Besland<sup>1</sup>, A. Gouillet<sup>1</sup>, M. Richard-Plouet<sup>1</sup>

<sup>1</sup>Université de Nantes, CNRS, Institut des Matériaux Jean Rouxel, IMN, F-44000 Nantes, France

<sup>2</sup>LAPLACE (Laboratoire Plasma et Conversion d'Énergie) ; Université de Toulouse ; CNRS, UPS, INPT; 118 route de Narbonne, F-31062 Toulouse cedex 9, France

## Abstract

Ti<sub>x</sub>Si<sub>1-x</sub>O<sub>2</sub> thin films appear as promising materials to replace SiO<sub>2</sub> for DRAM devices. For the effective down scaling, these mixed oxides should combine the best properties from SiO<sub>2</sub> (low leakage current) and TiO<sub>2</sub> (high dielectric constant). In this study, Ti<sub>x</sub>Si<sub>1-x</sub>O<sub>2</sub> thin films were deposited by low pressure PECVD. Varying the Titanium Tetra-Isopropoxide (TTIP) and Hexamethyldisiloxane (HMDSO) precursors flow rate allows us to obtain nanostructured films with tunable properties. Their surface chemical composition was assessed by X-ray Photoelectron Spectroscopy (XPS). Atomic Force Microscopy (AFM) revealed that the surface roughness increases with the Ti content. Spectroscopic Ellipsometry (SE) showed that a small amount of Ti is enough to induce a decrease of the energy gap and an increase of the refractive index, while preserving a low surface roughness. Since these mixed oxide films exhibit nanodomains with three different environments with randomly distributed Si-O-Ti bonds, SiO<sub>2</sub>-like and TiO<sub>2</sub>-like bonds, electrical properties are investigated at nanoscale in terms of dielectric permittivity, charge injection, trapping and transport via electrical modes derived from AFM as Electrostatic Force Microscopy (EFM), Kelvin Force Probe Microscopy (KPFM) and Conductive AFM (C-AFM). Despite a chemical composition evolving at the nanoscale, this work highlights that the electrical behavior can be considered as homogeneous (at the AFM resolution scale). A small amount of Ti induces a decrease in the amount of trapped electrons due to charge transport increase and a strong decrease of trapped holes. Moreover, after injection, the rate of charge decay increases with the Ti content. These features were interpreted on the basis of the energy diagrams deduced from the Valence Band measurement highlighting the n-type semiconducting character of the Ti-rich films. As a conclusion, Ti<sub>x</sub>Si<sub>1-x</sub>O<sub>2</sub> films with x=0.33 allows the best compromise in terms of dielectric permittivity improvement, charge injection and transport behavior.

## 1. Introduction

Nowadays, Internet of Things (IoT) and the Industry 4.0 have created a need for faster, smaller and lower energy demanding electronic systems aiming to support the cyber-physical systems. To address this demand, new direct random access memory (DRAM) generations aim in improving the access velocity and integration density. Concerning the storage capacitors, capacitance value should be increased while maintaining the leakage current density lower than  $10^{-8}$ - $10^{-7}$  A cm<sup>-2</sup> for 1 V applied bias voltage [1]. Several high-k materials were proposed (such as TiO<sub>2</sub>, ZrO<sub>2</sub>, HfO<sub>2</sub> or Ta<sub>2</sub>O<sub>5</sub>) enabling the down scaling of the DRAM with replacement of the SiO<sub>2</sub> layer with a physically thinner one [2]. This will maintain the same capacitance, but decrease the tunneling current. However, in most cases such metal oxides are subject to crystallization at low temperatures leading to polycrystalline films with rough interfaces [3].

To overcome this, the elaboration of mixed oxide films, exhibiting the most required properties from each oxide, was proposed by the scientific community. Among binary oxides, silicon (SiO<sub>2</sub>) and titanium (TiO<sub>2</sub>) dioxides are two promising candidates. On the one hand, SiO<sub>2</sub> is widely used in the semiconductor industry due to its low leakage current but associated to a low relative dielectric permittivity ( $\epsilon_r=3.9$ ), a refractive index  $n$  of 1.4 at 633 nm and an energy gap ( $E_g$ ) of 9 eV. On the other hand, TiO<sub>2</sub> is a highly investigated material exhibiting a high relative dielectric constant ( $\epsilon_r>50$ ) with the huge drawback of a high leakage current but associated to a higher refractive index  $n$  of 2.5 at 633 nm and an energy gap of 3.2 eV for the anatase phase [4]. Over the past decades, mixed oxide TiO<sub>2</sub>-SiO<sub>2</sub> films were investigated due to their promising optical [5], catalytic [6] or electrical [7] properties. TiO<sub>2</sub>-SiO<sub>2</sub> mixed oxide films have been implemented through several deposition techniques such as sol-gel [8-11], sputtering [5, 12-14], Chemical Vapor Deposition (CVD) [15-16], co-evaporation [17] and atmospheric or low pressure Plasma Enhanced Chemical Vapor Deposition (PECVD) [18-20]. The later one allows one to tune the film characteristics through the variation of experimental parameters such as gas mixture ratio or substrate type, and is well known for its high compatibility with microelectronics processes and micro-/nano- electronic devices. Among published results, several approaches were established. Recently, our group [19] investigated the growth conditions of the mixed oxide TiO<sub>2</sub>-SiO<sub>2</sub> thin films, elaborated at low pressure by PECVD. This previous study highlighted that by adjusting the precursor flow rates, non-columnar mixed TiO<sub>2</sub>-SiO<sub>2</sub> oxide films can be obtained.

Over the last years, the optical properties of ion-beam sputtered mixed oxide TiO<sub>2</sub>-SiO<sub>2</sub> films were examined in terms of chemical composition effect on the optical parameters such as

the optical energy gap and absorption level of the deposited films [5]. More recently, Larouche *et al.* [20], investigated the impact of the precursor ratio, in low pressure PECVD, on the chemical and optical characteristics of the film. Their results showed that the resulting one-phase material can be good candidate for graded-index optical filters. Several works of Brassard *et al.* [3, 21] investigated the importance of the oxygen flow rate and the impact of the substrate temperature, during deposition as well as during post-annealing, on the dielectric constant and electrical resistivity of the mixed oxide films, using various deposition techniques. The investigation of the composition effect of the mixed oxides  $Ti_xSi_{1-x}O_2$  was reported in a more recent work, where it was found that magnetron sputtered films, in reactive mode, not only exhibit high-k values but also low leakage current density as well [22].

To address applications, the knowledge of functional properties at nanoscale has a significant impact mainly due to down-scaling. In addition, as previously reported [23-24],  $TiO_2$  thin films can exhibit quite heterogeneous electrical properties at nanoscale. However, concerning the mixed oxides  $Ti_xSi_{1-x}O_2$  charge retention and transport properties remain poorly investigated, even at nanoscale, which affects the understanding of physical phenomena (carriers trapping and transport, charges exchange...) occurring at devices scale.

In this context, the objective of this work is to determine the evolution of the nanoscale electrical properties and optical characteristics of the mixed  $TiO_2$ - $SiO_2$  oxide film as a function of the chemical composition and to understand the relationship between different parameters. This was done combining structural, optical and nanoscale electrical characterizations. Indeed, in addition to structural investigations by Scanning Electron Microscopy (SEM), Atomic Force Microscopy (AFM) and X-ray Photoelectron Spectroscopy (XPS), optical characteristics were retrieved from spectroscopic ellipsometry (SE). The electrical properties were probed at the nanoscale by Electrostatic Force Microscopy (EFM) for dielectric permittivity, Kelvin Probe Force Microscopy (KPFM) and Conductive AFM (C-AFM) for charge injection, retention and transport, respectively.

## 2. Experiments

### 2.1. Materials

The mixed oxide  $TiO_2$ - $SiO_2$  thin films (50 nm thick), were obtained in a low-pressure PECVD reactor. A thickness of 50 nm was chosen, as a good compromise to address DRAM applications with an equivalent oxide thickness (EOT) of few nanometers, depending on dielectric permittivity [25]. The reactor comprises a diffusion chamber and a low-pressure high-

density Inductively Coupled plasma created at 13.56 MHz (400 W) via a helicon antenna. Oxygen is introduced at the top of the plasma source and a detailed description can be found in previous papers [26, 27]. The precursors used for the deposition of the mixed oxide layer were Titanium Tetra-Isopropoxide (TTIP) and Hexamethyldisiloxane (HMDSO) vapor respectively. The TTIP and HMDSO vapors, respectively at 84°C and 36°C, were introduced from the heated containers without a carrier gas through a distribution ring, located 8 cm above the substrate. In order to achieve pure inorganic films, the ratio of the precursor to the oxygen should be taken into consideration, as the oxygen atoms are the main species involved in the oxidation reactions, both in the plasma discharge and at the film surface [19]. During the deposition, the pressure value was set at 3 mTorr by adjusting the valve position of the turbo pump. A synopsis of the deposition parameters can be seen in Table 1. The variation of the TTIP and HMDSO flow rate was used to vary the Ti content in the deposited TiO<sub>2</sub>-SiO<sub>2</sub> mixed oxide films. SEM cross sectional views are difficult to prepare to ascertain a precise measurement of thickness equal to 50 nm. Moreover, the resolution of mechanical profilometry is also too low in that range of values. The films growth was therefore monitored with in situ ellipsometry with real-time fitting, hence allowing to stop deposition when the targeted thickness (50nm) was reached. Results were fitted again with great care afterwards, considering multiple models. Since we checked for higher thicknesses the soundness of the model we use, we are quite confident that the targeted thicknesses were achieved.

## 2.2. *Structural and surface characterization*

XPS on a Kratos Nova spectrometer with Al K $\alpha$  radiation at 1486.6 eV was used to investigate the chemical composition of the very surface. Wide range spectra were measured from 1200 eV to -2 eV (binding energy) using pass energy of 160 eV and high resolution core level spectra, with a pass energy of 40 eV. Differential charging effects were monitored by recording short scans (dwell times < 200 ms) and switching on the electron neutralizer during measurements. After applying a U2 Tougaard background, the decomposition in elemental components and fitting of the measured peaks were carried out using CasaXPS software [28] and Gaussian-Lorentzian functions. After calibration of the signal on the adventitious carbon at 285 eV, the Valence Band Maximum (VBM) is assessed from the offset of the curve intercepting the abscise axis. The Fermi level lies at 0 eV in binding energy. From different sets of experiments, the error in positioning VBM was estimated to 0.2 eV.

The mixed oxides' growth as well as their optical characteristics were monitored in situ through a rotating compensator ellipsometer (J.A. Woollam M-2000). The Spectroscopic Ellipsometry (SE) measurements were conducted in the 245 nm to 1000 nm wavelength range at  $71.7^\circ$  incident angle and fitting was performed using CompleteEASE software. The surface morphology of the thin films was checked using SEM and AFM with JEOL JSM 7600F in a secondary electron mode operating at 5 kV and with a Bruker Multimode 8 setup in tapping mode respectively.

### 2.3. Nanoscale electrical characterization

Nanoscale electrical characterizations were performed on a Bruker Multimode 8 setup with various modes. EFM measurements were done using Pt-coated Si-tip with resonance frequency  $f_0$  of 66.1 kHz, a quality factor  $Q$  of 293, a curvature radius  $R_c$  of 25 nm and a spring constant  $k$  of  $2.81 \text{ N m}^{-1}$ . EFM measurement of the resonance phase shift  $\Delta\phi_0$  was done at 20 nm-lift with an applied potential on the tip equal to 0 V or 5 V DC bias.

Measurements related to charge injection and decay were done, under controlled environment (without humidity and under  $\text{N}_2$  atmosphere), to avoid charges dissipation due to water layer presence on the sample surface [29]. The charging step was achieved in contact mode (contact force set to 20 nN to ensure tip-coating integrity) by applying positive or negative DC bias (from -40 V to +40 V by step of 10 V) to the AFM tip for 1 min, the sample back side being grounded. After this charging step, the same tip was used to probe the surface potential in Amplitude Modulation KPFM (AM-KPFM) mode using a 10 nm-lift. For surface potential measurement and charges injection protocol, a silicon AFM tip with PtIr coating ( $R_c = 25 \text{ nm}$  and  $k=2.43 \text{ N m}^{-1}$ ) is used.

Current measurements at nanoscale were performed with a PtIr coated Si-tip ( $R_c = 27 \text{ nm}$  and  $k = 0.4 \text{ N m}^{-1}$ ) using the Conductive AFM (C-AFM) mode with low noise amplifier modules. Different bias voltage was applied to the films as a function of film conductivity (from +/-5 V for  $\text{TiO}_2$  to +/-40 V for  $\text{SiO}_2$ ). The measurements were performed owing to the 100 nA/V module sensitivity for  $\text{TiO}_2$  film and the 20 pA/V module sensitivity for all the other films. During measurement a contact force of the cantilever on the sample of around 30 nN was used. This force ensures the tip-coating integrity.

### 3. Results

#### 3.1. Structural and surface characterization

In order to investigate the chemical composition of the mixed oxide thin films at the very surface, XPS measurements were carried out and the results are summarized in Table 1. In the first three columns, the flow rate of both precursors (HMDSO and TTIP) and the deposition rate are given. The atomic percentage of each element identified on the surface of the film, is indicated in the middle of the table, after the decomposition and fitting of the recorded peaks with CasaXPS software [28] and Gaussian-Lorentzian functions. As an example, the measured core level spectra (peaks) for one mixed film composition, are given in Fig. 1, for an HMDSO flow rate of 0.09 sccm and TTIP of 0.2 sccm.

**Table 1.** Evolution of deposition rate and  $Ti_xSi_{1-x}O_y$  chemical composition (from XPS analyses) as function of HMDSO and TTIP flow rates.

Flow rate (sccm)		Deposition rate (nm/min)	XPS atomic concentration (%)				Ti content	O content
HMDSO	TTIP		O	Ti	C	Si	x	y
0.33	0	7.9	63.7	0	5.53	30.7	0	2.07
0.16	0.2	5.3	54.7	8	20.8	16.6	0.33	2.05
0.09	0.2	3.1	53.8	12.2	21.4	12.6	0.49	1.99
0.07	0.36	3.6	52	12.5	24.7	10.8	0.54	2.08
0.07	0.7	4	46.5	20	31.2	2.7	0.89	2.15
0	0.2	1.1	52.5	23.5	23.8	0	1	2.20

For the Ti 2p and Si 2p levels (Fig. 1b and Fig. 1d respectively), we observe the typical spin-orbit splitting expected for 2p orbitales: i.e. two components 1/2 and 3/2 separated by 5 eV and 1eV for Ti 2p and Si 2p respectively [30]. The fitting of recorded peaks in elemental components allows us to identify the different chemical environments for each element. The binding energy positions for Ti 2p 3/2 at 459 eV and Si 2p 3/2 at 102.4 eV highlight that the Ti and Si atoms have only the 4+ oxidation degree, as expected for such films deposited by PECVD [30]. The atomic concentration of O 1s, Ti 2p, C 1s and Si 2p were determined from the peak areas moderated by the sensitivity factor of each level. On this basis, the atomic concentration is given in percentage directly in the corresponding Fig. 1 and in Table 1. In Fig. 1a, the O 1s core level appears constituted by three elemental components: the peak corresponding to the O-Si bond can be identified at the binding energy of 532.6 eV whereas the one corresponding to O-Ti is located at 530.5 eV. In-between these two peaks, another one can

be identified in position 531.5 eV which is known from our previous studies to correspond to Ti-O-Si bond. The three components correspond to the local arrangement of  $\text{TiO}_2$ ,  $\text{SiO}_2$  and main mixed environment of the O atoms as already reported [30]. Therefore, these specific mixed films can be notated as  $\text{Ti}_x\text{Si}_{1-x}\text{O}_y$ . Consequently, in the two last columns of Table 1, the Ti content (x) and O content (y) of the mixed films are provided.

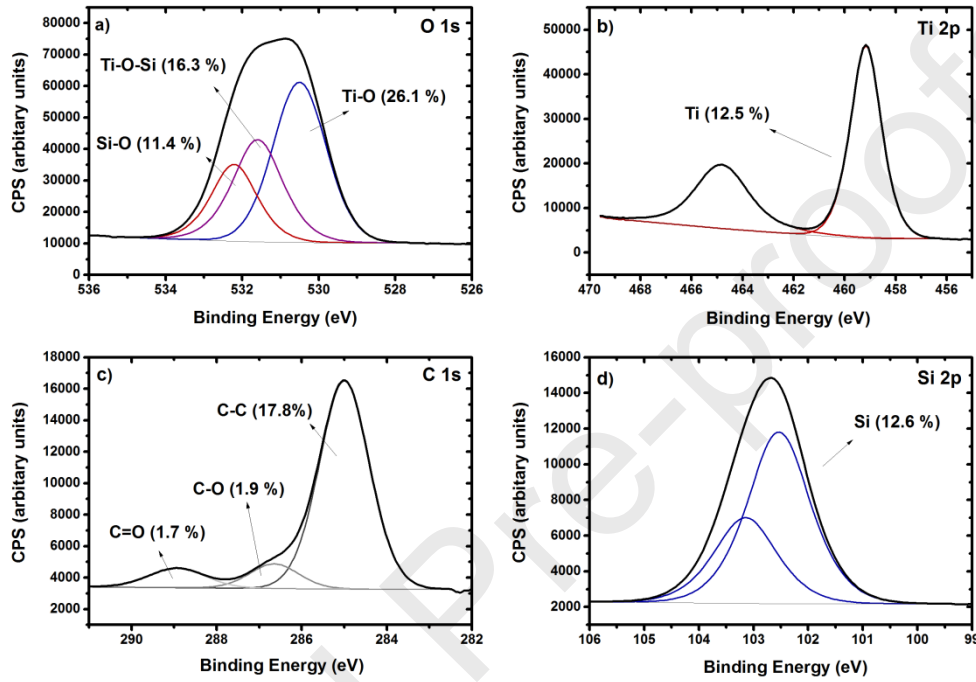


**Fig. 1.** XPS core level spectra of (a) O 1s, (b) Ti 2p, (c) C 1s and (d) Si 2p for the  $\text{Ti}_{0.49}\text{Si}_{0.51}\text{O}_2$  mixed oxide thin film measured by XPS.

As already described in previous work [19], the Ti atomic content can be calculated using the following formula:

$$x = \frac{[\text{Ti}]}{[\text{Ti}] + [\text{Si}]} \quad (1)$$

where [Ti] and [Si] are the atomic contents in titanium and silicon. In the same manner, the oxygen content can be calculated according to:

$$y = \frac{[\text{O}]}{[\text{Ti}] + [\text{Si}]} \quad (2)$$

Based on these equations, the x and y ratio for  $\text{Si}_x\text{Ti}_{1-x}\text{O}_y$  samples for different deposition conditions were determined (Table 1).

As expected, as the flow rate of HMDSO decreases compared to the TTIP one, the atomic Ti concentration in the film is increased. The carbon percentage shown in Table 1 is

mainly related to surface pollution. Indeed, previous studies have highlighted that carbon incorporation can be limited thanks to proper experimental conditions. Moreover, chemical analysis after soft etching of the very surface have shown that carbon was mainly related to surface contamination [31]. Due to the O-R (R=organic or hydroxyl groups), C-O and C=O bonds, the y ratio exceeds 2 mainly for Ti-rich films. Nonetheless, it lies in values close to the stoichiometric value of 2. As already reported, the Si-rich films usually exhibit a lower carbon content compared to Ti-rich films due to the lower carbon species per Si atom in HMDSO and their ability to be more efficiently oxidized in the O<sub>2</sub> plasma [4, 19]. Moreover, the ability of Ti cations to complex atmospheric carbon dioxide also contributes to the adsorption of carbon at the surface of the Ti-rich films. In case of  $x = 0.89$ , the relatively higher atomic percentage in carbon is related to the higher flow rate in TTIP. This is related to a technical limitation of our equipment regarding the minimal flow rate in HMDSO (0.07 sccm).

The surface morphology and topography of the deposited Ti<sub>x</sub>Si<sub>1-x</sub>O<sub>2</sub> thin films were investigated by SEM and AFM as reported in Fig. 2. From AFM height map measurement, the arithmetic average of the 3D roughness  $S_a$  was extracted. As expected, SiO<sub>2</sub> film exhibits low surface roughness  $S_a$  of 0.1 nm. Moreover, for TiO<sub>2</sub> film a rougher structure appears with a granular nanostructure [32] which is attributed to the columnar nanostructure arising at the surface [19]. The surface roughness  $S_a$  is higher, around 1.6 nm. Concerning Ti<sub>x</sub>Si<sub>1-x</sub>O<sub>2</sub> films ( $x = 0.89$  and below), the nanostructure morphology is less visible and the surface roughness  $S_a$  decreases to 0.7 nm and 0.2 nm for  $x = 0.89$  and  $x = 0.51$  respectively. For  $x = 0.49$  and below, the surface tends to be closer to smooth rather than granular with surface roughness around 0.1 nm for  $x = 0.49$  and  $x = 0.33$  similarly to a SiO<sub>2</sub> film.

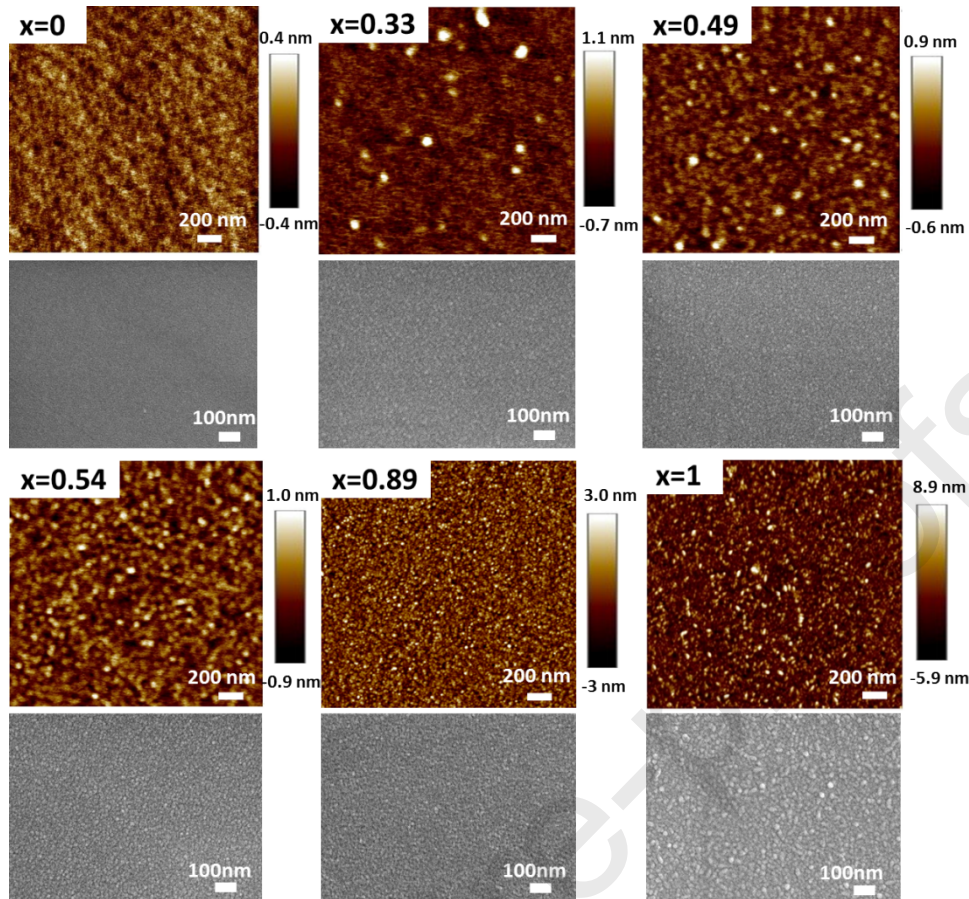


**Fig. 2.** AFM scans (colored) and SEM top view images (secondary electron) of the  $\text{Ti}_x\text{Si}_{1-x}\text{O}_2$  thin films for different  $x$  ratio.

### 3.2. Optical Characterization

The investigation of the optical and physical characteristics was carried out with spectroscopic ellipsometry based on the principle of the detection of change in polarization of incident light after reflection, probing two parameters named  $\psi$  and  $\Delta$ . These angles reflect change in amplitude and change in phase difference, respectively.

For the extraction of the film parameters and optical properties of interest, a model is needed in order to fit the measured data. For the pure  $\text{SiO}_2$  film ( $x = 0$ ), the Cauchy dispersion law was used, as it is more suitable for transparent amorphous films [33-34]. For the specific case of mixed oxide films, Li *et al.* [19] suggested to use the Tauc Lorentz (TL) dispersion law [35], which is well known to describe accurately the amorphous and nanocrystalline semiconductors optical constant in both the inter-band and the transparent regions. For the pure  $\text{TiO}_2$  film ( $x = 1$ ), it has been shown that the columnar structure affects the quality of the fit when a homogeneous model is used. To overcome this, a two-layer model with a dense  $\text{TiO}_2$

layer expressed with TL and a columnar one expressed with a graded layer composed of  $\text{TiO}_2$  and void has been proposed [4]. The schematic representation of these models can be seen in Fig. 3.a.

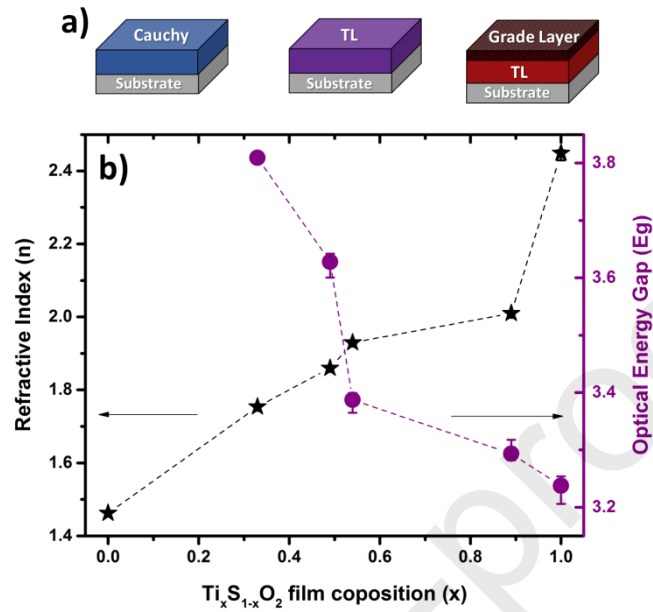


**Fig. 3.** a) Schematic representation of the models used to extract the ellipsometric parameters. b) Refractive Index ( $n$ ) at 633 nm (black stars) and Optical Energy Gap ( $E_g$ ) of  $\text{Ti}_x\text{Si}_{1-x}\text{O}_2$  films (purple circle).

By fitting the data with the proposed models, a wide variety of information such as the film thickness, the energy gap  $E_g$  and the refractive index  $n$  are extracted. The top roughness of the mixed oxides and the pure  $\text{SiO}_2$  film was not accounted for as it was found significantly low (lower than 1 nm). For the pure  $\text{TiO}_2$  film, surface roughness is modeled by the top of the graded layer as it accounts for 50% of  $\text{TiO}_2$  and 50% of void. The validity of each model is determined by the Mean Square Error (MSE) value, given in Table 2, which accounts for the discrepancies between the measured and simulated data. For all the fitted models, the MSE lies at around 10. In the case of  $x = 0.89$ , this value is slightly shifted to 14 which indicates that the uniform TL model tends to become relatively less suitable than for the other mixed films. Results summarized in Table 2, emphasize that all the  $\text{Ti}_x\text{Si}_{1-x}\text{O}_2$  films present thickness close to the targeted value (i.e. 50 nm). Fig. 3b indicates the variation of the refractive index  $n$  and optical  $E_g$  according to the mixed oxide composition. Concerning the refractive index  $n$ , a value of 1.47 and 2.44 was found for  $\text{SiO}_2$  and  $\text{TiO}_2$  films respectively which is close to values reported in the literature [24, 36]. Moreover, the refractive index is increased with the  $x$  ratio. So, verifying that by adjusting the precursor ratio and therefore the mixed oxide composition, the refractive index can be tuned accordingly. In the case of  $x = 0.89$ , a

lower value unexpected for a Ti-rich film is observed which could be a result of the used model, as described above. This quite low refractive index could be related to several parameters and the resulting value is a combination of those different effects: chemical composition of course but also film density (lower density will decrease the index), the amorphous or crystalline nature. In the case of  $x = 0$ , the optical  $E_g$  cannot be determined as it lies far from the range of measurement ( $E_g = 9$  eV from literature). As expected, the higher is the ratio of Si in the mixed oxide film, the higher is the  $E_g$ . Surprisingly, this observed gap increase remains at low level ( $E_g = 3.8$  eV for Si-rich film) compared to a  $\text{SiO}_2$  film (from literature). This leads to an interesting observation that as long as some incorporation of Ti takes place in the mixed oxide,  $E_g$  decreases and moves closer to the one of the  $\text{TiO}_2$ . Actually, as shown by DFT calculations for non-crystalline  $\text{Ti}_x\text{Si}_{1-x}\text{O}_2$  mixed oxides, increasing the Ti content leads to a reduction of the band gap independently on the amount of substituting species [37]. The DFT calculations have also shown that the decrease of the band gap with increasing Ti concentration in the  $\text{TiO}_2$ -rich region is mostly due to the increase of the overall Ti 3p-like valence bandwidth. Therefore, we infer that in the amorphous films prepared by PECVD the reduction of  $E_g$  with increasing Ti content may have the same origins.

**Table 2.** Thickness and optical gap ( $E_g$ ) determined by spectroscopic ellipsometry for various  $\text{Ti}_x\text{Si}_{1-x}\text{O}_2$  films. (used ellipsometry model is given in brackets)

$\text{Ti}_x\text{Si}_{1-x}\text{O}_2$ (x)	Thickness (nm)	Optical $E_g$ (eV)	MSE
0 (Cauchy)	51	-	5
0.33 (TL)	53	3.8	10
0.49 (TL)	45	3.7	9
0.54 (TL)	51	3.4	12
0.89 (TL)	50	3.3	14
1 (TL+ Grade)	25 + 31	3.2	8

### 3.3. Electrical characterization

The electrical properties of the deposited films were examined at the nanoscale range to extract further information. First of all, the relative dielectric permittivity was probed using EFM to identify possible heterogeneity in the material. Secondly, charge transport was investigated by C-AFM and charge injection and trapping by AM-KPFM.

First of all, relative dielectric permittivity could be determined using EFM measurements combined with Finite Element Modelling (FEM). This intends to determine the impact of the presence of TiO<sub>2</sub>-rich, SiO<sub>2</sub>-rich and mixed Si-O-Ti nanodomains, deduced from the interpretation of XPS data, on the local dielectric permittivity. [30]

EFM probe phase  $\Delta\phi_0$  (or frequency  $\Delta f_0$ ) shift of AFM tip induced by electrostatic force. This phase shift could be expressed as:

$$\Delta\phi_0 = -\frac{Q}{k} \cdot \text{grad}(F_e) \quad (3)$$

where Q is the quality factor, k the stiffness of the cantilever and F<sub>e</sub> the electrostatic force induced on AFM tip.

As the electrostatic force is proportional to the first derivative of capacitance with respect to the distance z, the phase shift  $\Delta\phi_0$  is directly correlated to the dielectric permittivity of the sample. In this study the dielectric permittivity of Ti<sub>x</sub>Si<sub>1-x</sub>O<sub>2</sub> layer was determined using the resonance phase shift  $\Delta\phi_0$  probed by EFM and a method derived from C. Riedel *et al.* [38].

From the experimental point of view, the resonance phase shift is probed at 0 V and 5 V, and the resulting phase shift parameter  $a_{\Delta\phi}$  is determined using the following equation:

$$a_{\Delta\phi} = \frac{\Delta\phi_0(5V) - \Delta\phi_0(0V)}{5^2 - 0^2} \quad (4)$$

This methodology permits to take into account a reference phase shift which corresponds to 0 V applied to the tip.

Images in Fig. 4 compare topography and phase shift parameter  $a_{\Delta\phi}$  map for Ti<sub>x</sub>Si<sub>1-x</sub>O<sub>2</sub> films surface with x = 0 (Fig. 4a and Fig. 4b) and for x = 0.54 (Fig. 4c and Fig. 4d). Whatever the Ti content, the phase shift appears homogeneous over the scanning area. To confirm this, the occurring diagram is depicted in Fig. 4e and represents the statistical repartition of phase shift parameter  $a_{\Delta\phi}$  over the scanning area. Pure SiO<sub>2</sub> and pure TiO<sub>2</sub> exhibit only one peak located at -0.43 °/V<sup>2</sup> and -0.71 °/V<sup>2</sup> respectively. Concerning Ti<sub>x</sub>Si<sub>1-x</sub>O<sub>2</sub> film with x=0.54, only one peak is observed located at -0.63 °/V<sup>2</sup> meaning that, at the scale of the AFM probe, the film is composed, at EFM-tip scale, by only one material and not a mixture of SiO<sub>2</sub> and TiO<sub>2</sub> separated phases. This was observed for all Ti<sub>x</sub>Si<sub>1-x</sub>O<sub>2</sub> film whatever Ti content. This is consistent with previous studies demonstrating that there is no crystallization evidence of TiO<sub>2</sub> grains within the bulk of TiO<sub>2</sub>-SiO<sub>2</sub> films [19, 32].

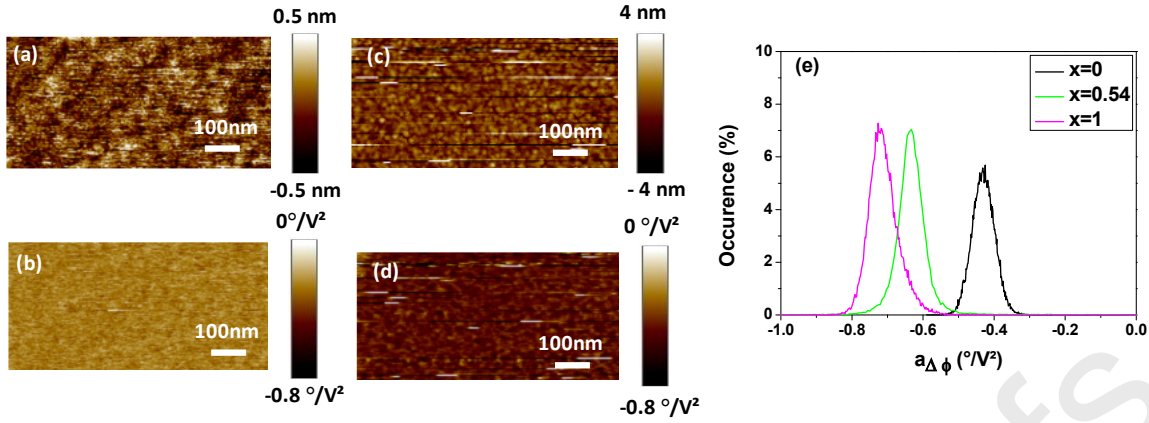


**Fig. 4.** (a) Topography and (b) phase shift  $a_{\Delta\phi}$  probed on  $\text{SiO}_2$  film by EFM. (c) Topography and (d) phase shift  $a_{\Delta\phi}$  probed on  $\text{Ti}_x\text{Si}_{1-x}\text{O}_2$  film with  $x=0.54$  by EFM. (e) Phase shift  $a_{\Delta\phi}$  occurrence diagram probed on  $\text{Ti}_x\text{Si}_{1-x}\text{O}_2$  films with various  $x$ .

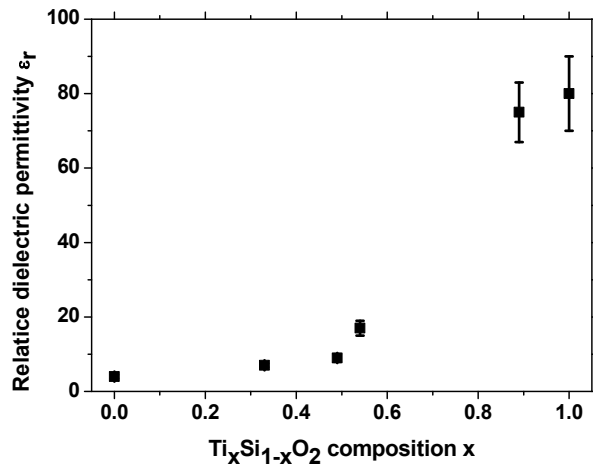
From a theoretical point of view, considering that the force gradient is related to the cantilever-tip-sample capacitance and that the latter is approximated as spring-mass system, the resonance phase shift  $a_{\Delta\phi}$  is related to the capacitance  $C$  between AFM probe and the sample by [38]:

$$a_{\Delta\phi} = \frac{Q}{2k'} \frac{d^2C}{dz^2} \quad (5)$$

where  $z$  is the vertical distance,  $Q$  the quality factor and  $k$  the stiffness of the cantilever.

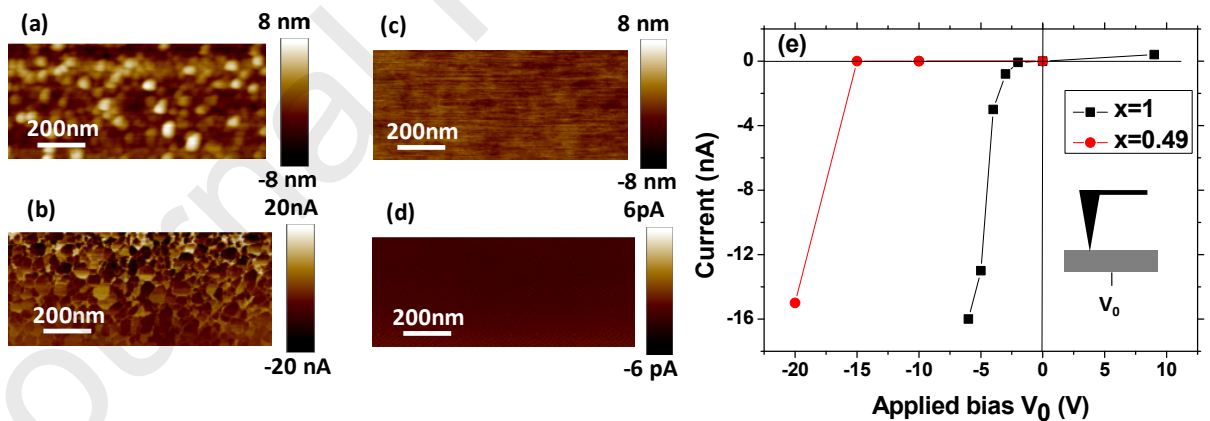
The quantity  $d^2C/dz^2$  is determined using a 2D axisymmetric FEM model on COMSOL [39], in which the electrostatic force  $F_e$  is computed at different lift positions and different dielectric permittivity values. This leads to a theoretical non-linear relationship between the relative dielectric permittivity  $\epsilon_r$  and  $a_{\Delta\phi}$ . It has to be noticed that the relation  $\epsilon_r = f(a_{\Delta\phi})$  is not linear and the slope increase with dielectric permittivity which impact the sensitivity at high dielectric permittivity.

Fig. 5 summarizes the evolution of the relative dielectric permittivity of  $\text{Ti}_x\text{Si}_{1-x}\text{O}_2$  films as function of  $x$ . A relative dielectric permittivity  $\epsilon_r$  of  $4 \pm 0.5$  and  $70 \pm 10$  is determined for  $\text{SiO}_2$  and  $\text{TiO}_2$  respectively which are close to the values previously reported in the literature [40]. A dispersion of around 14% is obtained from the occurrence profile width (Fig. 4e). Moreover, dielectric permittivity increases with the Ti content but remains far from the linear characteristic given by the mixing law, as from a thorough XPS study we identified that  $\text{Ti}_x\text{Si}_{1-x}\text{O}_2$  films are not formed of isolated  $\text{TiO}_2$  and  $\text{SiO}_2$  regions but are constituted of three different environments with randomly distributed Si-O-Ti bonds,  $\text{SiO}_2$ -like and  $\text{TiO}_2$ -like bonds [30].



**Fig. 5.** Evolution of the relative dielectric permittivity determined by EFM for  $Ti_xSi_{1-x}O_2$  films as function of  $x$ .

Secondly, charge transport in  $Ti_xSi_{1-x}O_2$  films were investigated at the nanoscale using C-AFM. In this configuration, the bias voltage is applied on the sample backside and current is collected by the AFM tip in contact with the  $Ti_xSi_{1-x}O_2$  films surface. This intends to identify preferential localization for charge transport in  $Ti_xSi_{1-x}O_2$  films, as those previously reported for  $TiO_2$  thin films [23-24].



**Fig. 6.** (a) Surface topography and (b) current map recorded for  $TiO_2$  film on Si substrate for -5V applied voltage  $V_0$ , (c) Surface topography and (d) current map recorded for  $Ti_xSi_{1-x}O_2$  ( $x = 0.49$ ) film on Si substrate for -15 V applied voltage. (e) Current variation versus applied voltage for two  $Ti_xSi_{1-x}O_2$  films for  $x = 1$  and  $x = 0.49$ . Inset, measurement configuration scheme.

Fig. 6a and Fig. 6b compare surface topography and current map for -5 V applied on  $TiO_2$  films. The current is not homogeneous and each grain appears more or less conductive. However, the

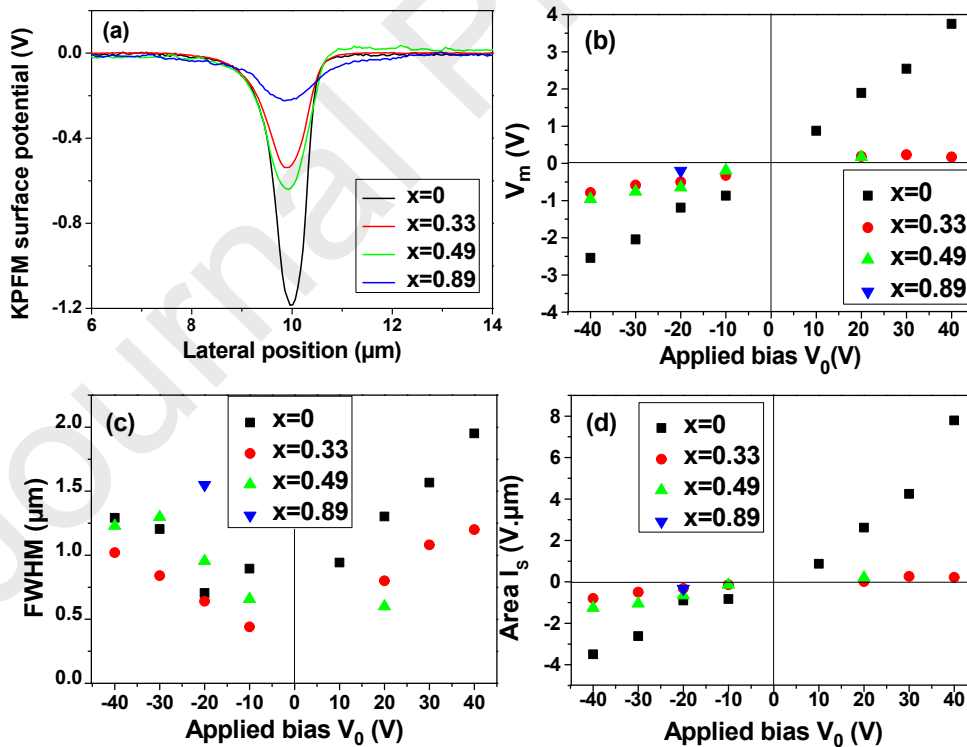
entire surface is conductive and a mean current value of -13 nA was detected for an applied voltage of -5 V. When positive bias of +5V is applied on TiO<sub>2</sub> films, a very low current is probed (only 50% of the surface appears conductive) and a mean current value of +50 pA was measured. For the SiO<sub>2</sub> film (not shown here), no current was detected from -40 V to 40 V, within the sensitivity limit of 30 fA of our instrument. These results are also in agreement with those reported in the literature for TiO<sub>2</sub> films obtained by MOCVD [24].

Fig. 6c and Fig. 6d compare surface topography and current map for -15V applied on Si<sub>1-x</sub>Ti<sub>x</sub>O<sub>2</sub> films with x = 0.49. The current is homogeneous over the whole scanning area and a mean current value of -0.2 pA, -2.2 pA and -15 nA was recorded for an applied voltage of -10 V, -15 V and -20 V respectively. When positive bias was applied to these films no current was detected. The same behavior was observed for all the Ti<sub>x</sub>Si<sub>1-x</sub>O<sub>2</sub> films with various Ti concentration: homogeneous current map and no current detected for positive bias up to 40 V. Moreover, the amount of current flowing through the films decreases with the increase of Si content. Indeed, a mean value for the current was found around -0.5 pA and -35 pA for -30 V and -35 V respectively applied to the mixed film with x = 0.33. Fig. 6e compares current evolution versus applied bias for two Ti<sub>x</sub>Si<sub>1-x</sub>O<sub>2</sub> films with x = 1 and x = 0.49. This confirms that for a fixed bias (i.e. electric field) the amount of current decreases with the increasing amount in Si.

Finally, to complete Ti<sub>x</sub>Si<sub>1-x</sub>O<sub>2</sub> films electrical properties characterization, charges injection and transport were investigated by AM-KPFM at local scale. In this configuration, charges were injected by applying a bias on the tip, whereas the Si substrate was grounded. A comparison of the resulting potential profiles, shown in Fig. 7a, reveals small differences between the four studied layers. Whatever the composition, stored charges remain close to the injection contact area. However, the amplitude of surface potential profile decreases with the Ti content. To accurately understand this behavior, surface potential profiles were fitted with a Gaussian shape function to extract three parameters: (i) maximum surface potential V<sub>m</sub>, (ii) the Full-Width at Half Maximum (FWHM) which represents the lateral charge spreading and (iii) the area under the potential peak I<sub>S</sub> which represents in a first approximation the charge density [39].

Concerning the SiO<sub>2</sub> film (black symbols), the maximum potential V<sub>m</sub> (Fig. 7b), the FWHM (Fig. 7c) and the area I<sub>S</sub> (Fig. 7d) linearly increase with applied bias for positive and negative injected carriers. Moreover, the amount of trapped charges is slightly higher for positive than for negative charge due to broader charge spreading. This behavior is consistent

with those previously reported in literature [29, 39]. For  $\text{Ti}_x\text{Si}_{1-x}\text{O}_2$  films with a small amount of Ti ( $x = 0.33$ , red symbols), a different behavior was observed for positive and negative charge. In case of electron injection, the maximum potential  $V_m$  (Fig. 7b), the FWHM (Fig. 7c) and the area  $I_s$  (Fig. 7d) linearly increase with applied bias, however the area  $I_s$  is lower which could imply that less charge density was trapped compared to  $\text{SiO}_2$ . In case of hole injection, the FWHM (Fig. 7c) increases with applied bias whereas the amount of injected and trapped charge remains low and a saturation is observed with applied bias increasing. The  $\text{Ti}_x\text{Si}_{1-x}\text{O}_2$  films (green symbols) with a middle-range amount of Ti ( $x = 0.49$  and  $x = 0.54$ ) also exhibit different behavior for positive and negative charge as previously. Concerning injected and trapped electron, the same behavior as for  $x = 0.33$  is observed. Concerning hole, the area under peak is small which seems to show that a small amount of charge is trapped and injected for  $x = 0.49$  at applied voltage of 10 V, whereas the film breakdown is observed for higher bias voltage. This tendency is confirmed for films with  $x = 0.89$  and  $x = 1$ . For  $x=0.89$ , the film breakdown is observed whatever positive bias voltage and for negative bias voltage higher than -20 V. For  $\text{TiO}_2$  film, the breakdown is observed whatever the applied bias voltage, this is probably related to the important measured current flow as shown in Fig. 6b and Fig. 6e.



**Fig. 7.** (a) Surface potential profile modification for a charge injection at -20V for 1 min in  $\text{Ti}_x\text{Si}_{1-x}\text{O}_2$  films. Evolution of maximum potential  $V_m$  (b), FWHM (c) and area  $I_s$  under KPFM surface potential peak (d) versus applied voltage during charge injection in  $\text{Ti}_x\text{Si}_{1-x}\text{O}_2$  films. Black, red, green and blue lines and symbols for  $x = 0, 0.33, 0.49$  and  $0.89$ , respectively.

To analyze charge transport after injection, the integrated intensity  $I_S$  and the potential profile FWHM were monitored as a function of the release time for each layer. To emphasize charge release dynamics, only normalized values are plotted as a function of time: (i) Normalized peak area  $I_n$  which corresponds to area at time  $t$  after injection divided by the initial area. (ii) Peak broadening  $\Delta W$  which corresponds to the difference between FWHM at time  $t$  and at  $t = 0$  s. The evolution of these two parameters is reported in Fig. 8. For each  $Ti_xSi_{1-x}O_2$  films, the same behavior is observed for electrons or holes whatever applied bias voltage. In addition, the normalized area  $I_n$  of the  $SiO_2$  film ( $x = 0$ ) remains quite constant, with a weak decrease after 2000 s (Fig. 8a), and the peak broadening  $\Delta W$  remains low (Fig. 8b). As a result, charge density is quite constant and only slow surface spreading is observed (lateral speed of  $75 \cdot 10^{-2} \text{ nm s}^{-1}$ ). Concerning  $Ti_xSi_{1-x}O_2$  films from small to middle-range Ti content (from  $x = 0.33$  to  $x = 0.54$ ), the normalized area  $I_n$  decreases quickly whereas the peak broadening remains low (same order as  $SiO_2$  film).  $I_S$  decrease rate is maximum during the first stage ( $< 500$  s) and is then reduced by a factor of 10. After 500 s, the decreasing rate of the area under peak and peak broadening are lower (lateral spreading speed  $75 \cdot 10^{-2} \text{ nm.s}^{-1}$ ). Concerning  $Ti_xSi_{1-x}O_2$  films with high Ti content ( $x = 0.89$ ), the normalized area  $I_n$  decreases quickly and the peak broadening is higher (lateral speed  $5 \text{ nm s}^{-1}$ ).

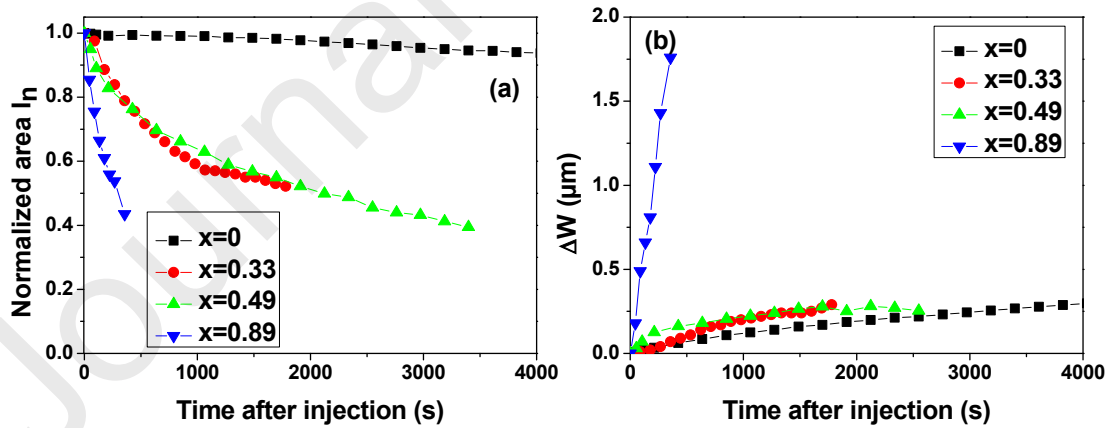


**Fig. 8.** (a) Evolution of (a) normalized area  $I_n$  and (b) peak broadening  $\Delta W$  as function of time after injection in  $Ti_xSi_{1-x}O_2$  films.

#### 4. Discussion

The results presented above demonstrate that a small amount of Ti induces strong modification of  $\text{Ti}_x\text{Si}_{1-x}\text{O}_2$  films morphological, optical and electrical properties. Moreover, only weak properties modification occurred, between  $x = 0.33$  and  $x = 0.49$ , compared to  $\text{SiO}_2$ .

To understand deeply these evolution, energy diagrams need to be investigated. To build it, the energy gap determined by SE and valence band measured by XPS were considered, after calibration of the signals on the adventitious carbon using XPS, the Fermi level lies at 0 eV in binding energy. From different sets of experiments, the error in positioning VBM was estimated to 0.2 eV. The VBM evolves from 5.1 eV for  $\text{SiO}_2$  ( $x = 0$ ) for which a gap of 9 eV was considered to 3.4 eV for  $x = 0.33$ , then to 3.0 eV when  $x$  increases to 0.54 and 2.9 eV and 2.8 eV to  $x = 0.89$  and  $x = 1$ , respectively. Using the energy gap  $E_g$ , the conduction band minimum (CBM) could also be determined. The resulting energy diagram is plotted in Fig. 9.

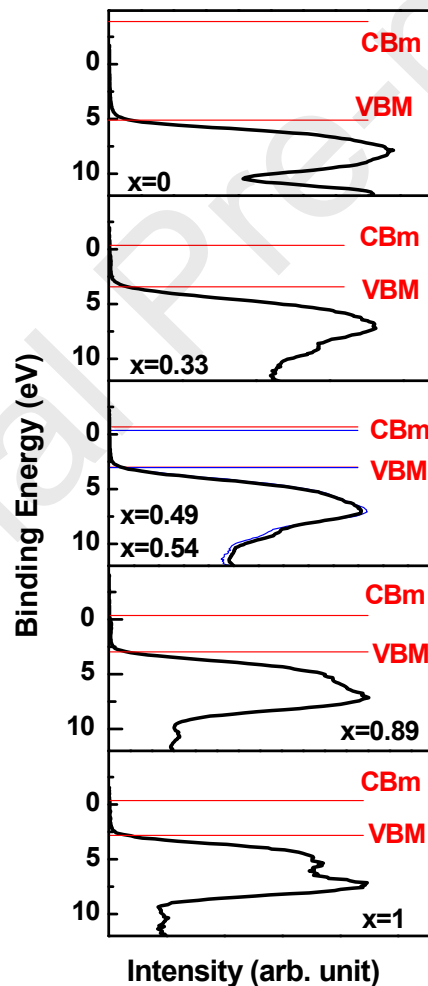


**Fig. 9.** Energy diagrams in Binding Energy with XPS signals calibrated according to C1s lying at 285 eV, from top to bottom  $x = 0$ ,  $x = 0.33$ ,  $x = 0.49$  &  $0.54$ ,  $x = 0.89$  and  $x = 1$ . While the experimental Valence Band is plotted in black, the Conduction Band Minimum (CBm) and Valence Band Maximum (VBM) are represented by red lines.

The results obtained for pure SiO<sub>2</sub> and TiO<sub>2</sub> films are in agreement with the expected ones. Concerning TiO<sub>2</sub>, the energy diagram is typical for a n-type semi-conductor with the Fermi level lying very close to the CBm. Since the VBM lies at 2.8 eV below the Fermi level, the CBm is situated at 0.6 eV above the latter. Usually the electron affinity of TiO<sub>2</sub> is 4.2 eV with respect to the vacuum level, meaning that the Fermi level lies at -4.8 eV. The work function of the PtIr tip was measured at to -5.6 eV. Therefore, the difference with this value is 0.8 eV and induces the formation of a Schottky barrier when the tip is contacted with the film. This explains the n-type diode behavior observed on C-AFM current versus voltage characteristic, with a blocking (passing) diode behavior applying positive (negative) DC voltage on Si substrate (Fig. 6e). Moreover, this also explains the fact that no carrier could be trapped in TiO<sub>2</sub>. Indeed, all injected charges are transported through the film. Concerning SiO<sub>2</sub> film, with the Fermi level lying in the middle of the gap, the SiO<sub>2</sub> film exhibits an insulating character. The large band gap value is in agreement with no current probed by C-AFM even at high electric field. Moreover, the charges injected into the SiO<sub>2</sub> film are trapped close to the injection area and remained trapped a long time after injection, thanks to its good insulating properties. The electron affinity of silica is generally reported to be equal to 1.1 eV. Since the Fermi level of silica lies in the middle of the gap, it is located at -5.6 eV with respect to vacuum level. With the work function of the PtIr tip measured at to -5.6 eV, those two levels are aligned explaining why electrons and holes present the same injection behavior.

More surprisingly, Ti<sub>x</sub>Si<sub>1-x</sub>O<sub>2</sub> films, even with a small amount of Si, exhibit an energy diagram typical for a n-type semi-conductor with a Fermi level very close to the CBm. This could explain the evolution of the current versus voltage characteristics obtained by C-AFM for Ti<sub>x</sub>Si<sub>1-x</sub>O<sub>2</sub> films with  $x = 0.46$  (Fig. 6e). Indeed, we observe a n-type diode behavior, similarly to TiO<sub>2</sub> films, but with higher threshold voltage. Considering films with low Ti content, the current flow through the films is in the same range than dielectric material. Indeed, for Ti<sub>x</sub>Si<sub>1-x</sub>O<sub>2</sub> films with  $x = 0.33$ , a current of -2.2 pA is probed for a mean electric field of  $-3.10^8$  V m<sup>-1</sup> (i.e. 15 V applied on 50 nm) whereas, in the literature, it was reported 50 pA on a-SiO<sub>x</sub>N<sub>y</sub> ( $\gamma=5$ ) films under mean electric field of  $6.10^7$  V m<sup>-1</sup> (i.e. 10 V applied on 165 nm) [29]. This could imply that Ti<sub>x</sub>Si<sub>1-x</sub>O<sub>2</sub> ( $0 < x < 1$ ) films exhibit a very low conductivity for a n-type semiconductor. Concerning charge injection and trapping in Ti<sub>x</sub>Si<sub>1-x</sub>O<sub>2</sub> films, different behaviors were observed for electrons and holes injection. Indeed, the amount of trapped holes is lower than the electrons one. This dissymmetry can also be explained considering the energy diagram (Fig. 9) and current through the film. Indeed, as for TiO<sub>2</sub> film, the tip work function is closer to CBm which

should favor electrons injection and limit hole injection. Concerning electrons, whatever the Ti content during carrier injection a steady state is probably reached between charge injection and transport due to significant current flow. This implies that electrons could be trapped in the volume far from the surface. From a theoretical point of view, when charge distribution spreads in depth, a higher quantity of charge is needed to lead to the same surface potential. So, a decrease of surface potential observed with Ti content increasing could be linked to a broader distribution of charge within the dielectric film thickness. To confirm such hypothesis a 3D charge density probing method is needed to investigate deeper the charge injection mechanism and identify charge penetration depth and the amount of injected charge.

Finally, in term of devices applications  $Ti_xSi_{1-x}O_2$  films with  $x = 0.33$  stand as a good compromise between dielectric permittivity enhancement (twice than  $SiO_2$  one), lower charge injection than  $SiO_2$  but a current flow lower than for other Ti content (-35 pA at -35 V). However, as a perspective to this purpose, another interesting design would be the implementation of nanocomposite films incorporating  $TiO_2$  nanoparticles in a  $SiO_2$  matrix. Hence the semi-conducting character could be tuned through the degree of percolation of the nanoparticles.

## 5. Conclusion

In this paper tunable electrical properties of  $Ti_xSi_{1-x}O_2$  films deposited by PECVD were investigated at nanoscale in term of dielectric permittivity, charge injection, trapping and transport. Adjusting TTIP and HMDSO flow rate during plasma deposition allows us to obtain films with tunable properties. Considering local electrical measurement, the obtained materials are homogeneous single phase without evidence of Ti-rich or Si-rich regions.

The Ti amount increasing induces a weak increasing of surface roughness, a decreasing of optical energy gap and a non-linear increasing of the dielectric permittivity. Concerning charge injection and trapping, for  $SiO_2$  films, holes and electrons are injected with the same dynamics and charges remain trapped close to the injection point. XPS and SE results demonstrate that  $Ti_xSi_{1-x}O_2$  films ( $x > 0.33$ ) have an n-type behavior which explains the quite high amount of current probed by C-AFM. Moreover, the amount of trapped electrons seems to be higher than holes, but remains lower than  $SiO_2$ . Indeed, electron trapping is limited by carrier transport through the film, and a steady state regime is obtained between injection and transport phenomena.

From the device applications point of view,  $\text{Ti}_x\text{Si}_{1-x}\text{O}_2$  films with  $x = 0.33$  stand as a good compromise between dielectric permittivity enhancement and a moderate increasing of current flow compared to  $\text{SiO}_2$ .

So, the perspectives of this work are both. To go further in understanding of charge injection, trapping and transport mechanisms in  $\text{Ti}_x\text{Si}_{1-x}\text{O}_2$  films, space charge density needs to be probed in 3D. Moreover, concerning devices applications,  $\text{TiO}_2$ - $\text{SiO}_2$  nanocomposite, with different load in  $\text{TiO}_2$  nanoparticles, should be investigated to evaluate the impact of controlled nanostructuration on dielectric permittivity, charge trapping and transport.

### Acknowledgements

This work was financially supported by the French GDR SEEDS.

### References

- [1] S. K. Kim, G.J. Choi, S.Y. Lee, M. Seo, S.W. Lee, J.H. Han, H.S. Ahn, S. Han and C.S. Hwang, Al-doped  $\text{TiO}_2$  films with ultralow leakage currents for next generation DRAM capacitors, *Adv. Mat.* 20 (2008) 1429, <https://doi.org/10.1002/adma.200701085>
- [2] Y.C. Yeo, T.J. King. and C. Hu , Direct tunneling leakage current and scalability of alternative gate dielectrics, *Appl. Phys. Lett.* 81 (2002) 2091, <https://doi.org/10.1063/1.1506941>
- [3] D. Brassard, D.K. Sarkar, M.A. El Khakani and L. Ouellet, High- $k$  titanium silicate thin films grown by reactive magnetron sputtering for complementary metal–oxide–semiconductor applications, *J. Vac. Sci. Technol. A* 22 (2004) 851, <https://doi.org/10.1116/1.1722530>.
- [4] D. Li, M. Carette, A. Granier, J.P. Landesman and Goullet A, In situ spectroscopic ellipsometry study of  $\text{TiO}_2$  films deposited by plasma enhanced chemical vapour deposition, *Appl. Surf. Sci.* 283 (2013) 234, <https://doi.org/10.1016/j.apsusc.2013.06.091>
- [5] H. Demiryont, Optical properties of  $\text{SiO}_2$ – $\text{TiO}_2$  composite films, *Appl. Opt.* 24 (1985) 2647, <https://doi.org/10.1364/AO.24.002647>
- [6] F. Gracia, F. Yubero, J.P. Espinos, J.P. Holgado, A.R. Gonzalez-Elipse and T. Girardeau, Correlation between optical properties and electronic parameters for mixed oxide thin films, *Surf. Interface Anal.* 38 (2006) 752, <https://doi.org/10.1002/sia.2273>
- [7] C. Anderson and A.J. Bard, Improved photocatalytic activity and characterization of mixed  $\text{TiO}_2/\text{SiO}_2$  and  $\text{TiO}_2/\text{Al}_2\text{O}_3$  materials, *J. Phys. Chem. B* 101 (1997) 2611, <https://doi.org/10.1021/jp9626982>
- [8] S. Kermadi, N. Agoudjil, S. Sali, L. Zougar, M. Boumaour, L. Broch, A. En Naciri and F. Placido, Microstructure and optical dispersion characterization of nanocomposite sol-gel  $\text{TiO}_2$ - $\text{SiO}_2$  thin films with different compositions, *Spectrochim. Acta. A. Mol. Biomol. Spectrosc.* 145 (2015) 145, <https://doi.org/10.1016/j.saa.2015.02.110>

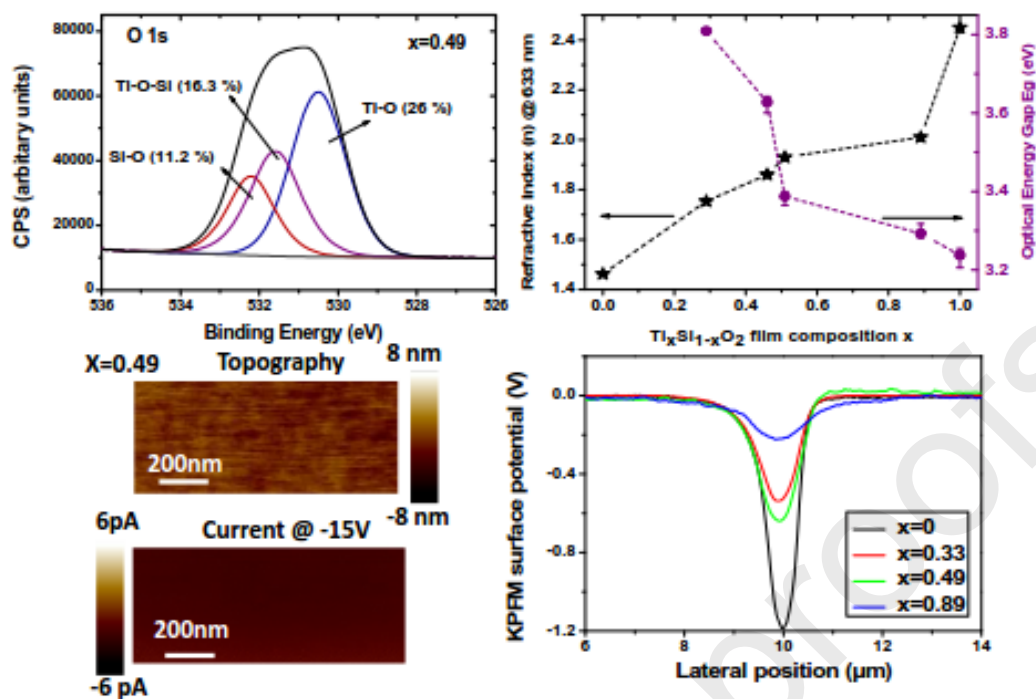
- [9] D. K. Sarkar, D. Brassard, M.A.E. Khakani and L. Ouellet, Dielectric properties of sol-gel derived high-k titanium silicate thin films, *Thin Solid Films*, 515 (2007) 4788, <https://doi.org/10.1016/j.tsf.2006.11.155>
- [10] D.K. Sarkar, D. Brassard, M.A. El Khakani and L. Ouellet, Single-electron tunneling at room temperature in  $Ti_xSi_{1-x}O_2$  nanocomposite thin films, *Appl. Phys. Lett.* 87 (2005) 253108, <https://doi.org/10.1063/1.2147729>
- [11] P.H. Giauque, H.B. Cherry and M.A. Nicolet, Thermal stability of amorphous  $Ti_3Si_1O_8$  thin films, *Microelectron. Eng.* 55 (2001) 183, [https://doi.org/10.1016/S0167-9317\(00\)00446-9](https://doi.org/10.1016/S0167-9317(00)00446-9)
- [12] X. Wang, H. Masumoto, Y. Someno and T. Hirai, Microstructure and optical properties of amorphous  $TiO_2$ - $SiO_2$  composite films synthesized by helicon plasma sputtering, *Thin Solid Films* 338 (1999) 105, [https://doi.org/10.1016/S0040-6090\(98\)01007-4](https://doi.org/10.1016/S0040-6090(98)01007-4)
- [13] S. Chao, W.H. Wang, M.Y. Hsu and L.C. Wang, Characteristics of ion-beam-sputtered high-refractive-index  $TiO_2$ - $SiO_2$  mixed films, *J. Opt. Soc. Am. A* 16 (1999) 1477, <https://doi.org/10.1364/JOSAA.16.001477>
- [14] D. Brassard and M.A. El Khakani, Thermal behavior of the microstructure and the electrical properties of magnetron-sputtered high-k titanium silicate thin films, *J. Appl. Phys.* 103 (2008) 114110, <https://doi.org/10.1063/1.2937241>
- [15] S.M. Lee, J.H. Park, K.S. Hong, W.J. Cho and D.L. Kim, The deposition behavior of  $SiO_2$ - $TiO_2$  thin film by metalorganic chemical vapor deposition method, *J. Vac. Sci. Technol. A*. 18 (2000) 2384, <https://doi.org/10.1116/1.1287154>
- [16] A. Paskaleva, A.J. Bauer, M. Lemberger and S. Zürcher, Different current conduction mechanisms through thin high-k  $Hf_xTi_ySi_zO$  films due to the varying Hf to Ti ratio, *J. Appl. Phys.* 95 (2004) 5583, <https://doi.org/10.1063/1.1702101>
- [17] J.S. Chen, S. Chao, J. S. Kao, H. Niu and C. H. Chen, Mixed films of  $TiO_2$ - $SiO_2$  deposited by double electron-beam coevaporation, *Appl. Opt.* 35 (1996) 90, <https://doi.org/10.1364/AO.35.000090>
- [18] Y. Gazal, C. Dublanche-Tixier, A. Antoine, M. Colas, C. Chazelas and P. Tristant, Elaboration of nanostructured  $TiO_2/SiO_2$  films by plasma enhanced chemical vapor deposition at atmospheric pressure, *Thin Solid Films* 619 (2016) 137, <https://doi.org/10.1016/j.tsf.2016.11.010>
- [19] D. Li, S. Elisabeth, A. Granier, M. Carette, A. Goulet and J.P. Landesman, Structural and optical properties of PECVD  $TiO_2$ - $SiO_2$  mixed oxide films for optical applications, *Plasma Process. Polym.* 13 (2016) 918, <https://doi.org/10.1002/ppap.201600012>
- [20] S. Larouche, H. Szymanowski, J.E. Klemberg-Sapieha, L. Martinu and S.C. Gujrathi, Microstructure of plasma-deposited  $SiO_2/TiO_2$  optical films, *J. Vac. Sci. Technol.* 22 (2004) 1200, <https://doi.org/10.1116/1.1763912>
- [21] D. Brassard and M.A. El Khakani, Pulsed-laser deposition of high-k titanium silicate thin films, *J. Appl. Phys.* 98 (2005) 054912, <https://doi.org/10.1063/1.2039274>
- [22] D. Brassard, D.K. Sarkar, M.A. El Khakani and L. Ouellet, Compositional effect on the dielectric properties of high-k titanium silicate thin films deposited by means of a co-sputtering process, *J. Vac. Sci. Technol. A* 24 (2006) 600, <https://doi.org/10.1116/1.2180267>
- [23] K. Murakami, M. Rommel, B. Hudec, A. Rosova, K. Husekova, E. Dobrocka, R. Rammula, A. Kasikov, J.H. Han, W. Lee, S.J. Song, A. Paskaleva, A.J. Bauer, L. Frey, K. Frohlich, J. Aarik and C.S. Hwang, Nanoscale Characterization of  $TiO_2$  Films Grown by Atomic Layer Deposition on  $RuO_2$  Electrodes, *Appl. Mat. Interfaces* 6 (2014) 2486, <https://doi.org/10.1021/am4049139>

- [24] A. Miquelot, O. Debieu, V. Rouessac, C. Villeneuve, N. Prud'homme, J. Cure, V. Constantoudis, G. Papavieros, S. Roualdes and C. Vahlas, TiO<sub>2</sub> nanotree films for the production of green H<sub>2</sub> by solar water splitting: From microstructural and optical characteristics to the photocatalytic properties, *Applied Surface Science* 494 (2019) 1127, <https://doi.org/10.1016/j.apsusc.2019.07.191>
- [25] J.A. Kittl, K. Opsomer, M. Popovici, N. Menou et al, High-k dielectrics for future generation memory devices, *Microelec. Eng.* 86 (2009) 1789, <https://doi.org/10.1016/j.mee.2009.03.045>
- [26] F. Nicolazo, A. Goulet, A. Granier, C. Vallée, G. Turban and B. Grolleau, Study of oxygen/TEOS plasmas and thin SiO<sub>x</sub> films obtained in a helicon diffusion reactor, *Surf. Coat. Technol.* 98 (1998) 1578, [https://doi.org/10.1016/S0257-8972\(97\)00295-8](https://doi.org/10.1016/S0257-8972(97)00295-8)
- [27] A. Granier, F. Nicolazo, C. Vallée, A. Goulet, G. Turban and B. Grolleau, Diagnostics in O<sub>2</sub> helicon plasmas for SiO<sub>2</sub> deposition, *Plasma Sources Sci. Technol.* 6 (1997) 147, <http://iopscience.iop.org/0963-0252/6/2/008>
- [28] Neal Fairley, *Copyright© 2005 Casa Software Ltd* (2005).
- [29] C. Villeneuve-Faure, K. Makasheva, C. Bonafos, B. Despax, L. Boudou, P. Pons and G. Teyssedre, Kelvin force microscopy characterization of charging effect in thin a-SiO<sub>x</sub>N<sub>y</sub>:H layers deposited in pulsed plasma enhanced chemical vapor deposition process by tuning the silicon environment, *J. Appl. Phys.* 113 (2013) 204102, <https://doi.org/10.1063/1.4795721>
- [30] P. Ondračka, D. Nečas, M. Carette, S. Elisabeth, D. Holec, A. Granier, A. Goulet, L. Zajíčková, M. Richard-Plouet, Unravelling local environments in mixed TiO<sub>2</sub>-SiO<sub>2</sub> thin films by XPS and ab initio calculations, *Appl. Surf. Sc.* 510 (2020) 145056, <https://doi.org/10.1016/j.apsusc.2019.145056>
- [31] S. Elisabeth, "Elaboration de couches minces diélectriques d'oxydes de titane et silicium à forte permittivité et indice optique par procédé plasma PECVD basse pression", PhD of Nantes University, 2015, <https://www.theses.fr/220165262>
- [32] A. Borrás, R. Alvarez, J.R. Sanchez-Valencia, J. Ferrer and A.R. Gonzalez-Elipe, Critical thickness and nanoporosity of TiO<sub>2</sub> optical thin films, *Microporous Mesoporous Mater.* 160 (2012) 1, <https://doi.org/10.1016/j.micromeso.2012.04.035>
- [33] H.G. Tompkins, editor, *Handbook of Ellipsometry*, Repr (Andrew [u.a.], Norwich, NY, 2010).
- [34] C.M. Herzinger, B. Johs, W.A. McGahan, J.A. Woollam, W. Paulson, Ellipsometric determination of optical constants for silicon and thermally grown silicon dioxide via a multi-sample, multi-wavelength, multi-angle investigation, *J. Appl. Phys.* 83 (1998) 3323, <https://doi.org/10.1063/1.367101>
- [35] G.E. Jellison and F.A. Modine, Parameterization of the optical functions of amorphous materials in the interband region, *Appl. Phys. Lett.* 69 (1996) 371, <https://doi.org/10.1063/1.118064>
- [36] I. H. Malitson, Interspecimen comparison of the refractive index of fused silica, *J. Opt. Soc. Am.* 55 (1965) 1205, <https://doi.org/10.1364/JOSA.55.001205>
- [37] P. Ondračka, D. Holec, D. Necas, E. Kedronova, S. Elisabeth, A. Goulet, L. Zajickova, Optical properties of TixSi1-xO2 solid solutions, *Phys. Rev. B.* 95 (2017) 195163. <https://doi.org/10.1103/PhysRevB.95.195163>.
- [38] C. Riedel, R. Arinero, Ph. Tordjeman, M. Ramonda, G. Lévêque, G.A. Schwartz, D.G. de Oteyza, A. Alegria and J. Colmenero, Determination of the nanoscale dielectric constant by means of a double pass method using electrostatic force microscopy, *J. Appl. Phys.* 106 (2009) 024315, <https://doi.org/10.1063/1.3182726>
- [39] C. Villeneuve-Faure C, K. Makasheva K, L. Boudou L and G. Teyssedre, Charge injection in thin dielectric layers by atomic force microscopy: influence of geometry and material work function of the

AFM tip on the injection process, Nanotechnology 27 (2016) 245702, <https://doi.org/10.1088/0957-4484/27/24/245702>

[40] J. Robertson, High dielectric constant oxides, Eur. Phys. J. Appl. Phys. 28 (2004) 265, <https://doi.org/10.1051/epjap:2004206>

Journal Pre-proofs



**Highligh**

- TiO<sub>2</sub>-SiO<sub>2</sub> mixed oxide films deposited by PECVD, with tunable properties from SiO<sub>2</sub> to TiO<sub>2</sub> ones.
- Relationship between material heterogeneity at atomic scale and electrical properties at nanoscale.
- Investigation of dielectric permittivity, charge injection, trapping and transport as function of the [Ti]/([Ti]+[Si]) content.
- A small amount of Ti strongly influences properties as optical gap, charge injection, trapping and transport.
- Concerning applications, the best compromise between high dielectric permittivity and low current flow is obtained for x=0.33.

**M. Mitronika** : Resources, Investigation, Methodology, Writing - Original Draft

**C. Villeneuve-Faure** : Investigation, Methodology, Conceptualization, Writing - Original Draft, Writing - Review & Editing

**F. Massol** : Investigation

**L. Boudou** : Conceptualization, Writing - Review & Editing

**W. Ravisy** : Investigation, Writing - Review & Editing

**M.P. Besland** : Conceptualization, Writing - Review & Editing

**A. Goulet** : Resources, Methodology, Conceptualization, Writing - Review & Editing

**M. Richard-Plouet** : Investigation, Methodology, Conceptualization, Writing - Review & Editing

Journal Pre-proofs

**Declaration of interests**

The authors declare that they have no known competing financial interests or personal relationships that could have appeared to influence the work reported in this paper.

The authors declare the following financial interests/personal relationships which may be considered as potential competing interests:

Journal Pre-proofs